Earth's Future

RESEARCH ARTICLE
10.1029/2024EF005256

Concurrent Heat Extremes in Relation to Global Warming, High Atmospheric Pressure and Low Soil Moisture in the Northern Hemisphere

Dalai Nasong[1,2], Sha Zhou[1,2], Kai Kornhuber[3,4,5], and Bofu Yu[6]

[1]State Key Laboratory of Earth Surface Processes and Resource Ecology, Faculty of Geographical Science, Beijing Normal University, Beijing, China, [2]Faculty of Geographical Science, Institute of Land Surface System and Sustainable Development, Beijing Normal University, Beijing, China, [3]Lamont-Doherty Earth Observatory, Columbia University, New York, NY, USA, [4]Climate Analytics, Berlin, Germany, [5]Potsdam Institute for Climate Impact Research, Potsdam, Germany, [6]School of Engineering and Built Environment, Griffith University, Nathan, QLD, Australia

Key Points:

- Concurrent heat extremes have increased greatly in the Northern Hemisphere since 1950
- Global warming drives long-term increases in the frequency and strength of concurrent heat extremes, particularly in the tropics
- Concurrent high atmospheric pressure primarily influences temporal and spatial variations in concurrent heat extremes in mid-latitudes

Correspondence to:
S. Zhou,
shazhou21@bnu.edu.cn

Citation:
Nasong, D., Zhou, S., Kornhuber, K., & Yu, B. (2025). Concurrent heat extremes in relation to global warming, high atmospheric pressure and low soil moisture in the Northern Hemisphere. *Earth's Future*, *13*, e2024EF005256. https://doi.org/10.1029/2024EF005256

Received 5 APR 2024
Accepted 9 DEC 2024

Abstract Summer heat extremes increasingly co-occur worldwide, posing disastrous impacts on our society and the environment. However, the spatial pattern and underlying mechanisms of concurrent heat extremes remain unclear. We used a statistical framework to estimate the spatial concurrence strength of heat extremes in the Northern Hemisphere and identified their relationships to global warming, atmospheric circulation, and land-atmosphere feedbacks. Concurrent heat extremes over different regions have significantly increased in the Northern Hemisphere from 1950 to 2023. Moreover, heat extremes show strong spatial concurrence strength, and the driving factors vary geographically. Global warming is responsible for long-term increases in the frequency and strength of concurrent heat extremes, with most pronounced impact in tropical regions. In the absence of warming trends, the temporal and spatial variations in concurrent heat extremes are mainly caused by simultaneous high atmospheric pressure controlled by large-scale circulations, particularly in mid-latitude regions. While low soil moisture enhances regional heat extremes through land-atmosphere feedbacks, it plays a minor role in driving concurrent heat extremes alone but can contribute in combination with high-pressure anomalies. Given the ever-increasing risks of heat extremes, our study underscores the importance of identifying the mechanisms of spatially concurrent heat extremes to improve prediction and mitigation of widespread heatwaves and their adverse impacts on socio-economic sustainability and human well-being.

Plain Language Summary Increases in concurrent heat extremes across different regions of the world pose significant threats to communities and ecosystems. Understanding the spatial pattern of heat extremes and their underlying mechanisms is crucial for mitigating the adverse effects and adapting to future occurrences of heat extremes. While previous studies have focused on local drivers of heat extremes, the influences of various drivers on the concurrence of heat extremes across different regions remain unclear. Our study shows that global warming has strengthened the spatial concurrence of heat extremes, particularly over the tropics. Concurrent high atmospheric pressure, propelled by large-scale circulation anomalies, are largely responsible for the spatial concurrence of heat extremes in mid-latitudes. Additionally, land-atmosphere feedbacks amplify local heat extremes and influence spatially concurrent heat extremes in conjunction with high-pressure anomalies over different regions. Our enhanced mechanistic understanding of the spatial concurrence of heat extremes will inform effective strategies and practices to mitigate and adapt to future risks of heat extremes.

1. Introduction

Global warming has increased occurrence of heat extremes in many parts of the world, which pose serious threat to socio-economic development, human health, and ecosystem sustainability (Bastos et al., 2020; García-León et al., 2021; Lüthi et al., 2023; Song et al., 2024). A record-breaking extreme heatwave exceeding five standard deviations caused hundreds of deaths, horrific wildfires, and the death of various wild animals and plants in western North America in 2021 (Thompson et al., 2022; White et al., 2023). The unprecedented heatwave of 2022 in China and India had inflicted widespread impacts, including a surge of heat-related illnesses and deaths, substantial agricultural losses, environmental degradation, infrastructure damage, and significant economic disruptions (Sidhu, 2023; Xu et al., 2024). In recent years, the frequency, intensity, persistence, and spatial extent

of heat extremes have increased significantly (Domeisen et al., 2023; Perkins-Kirkpatrick & Lewis, 2020). In addition, concurrent heat extremes have increased across large areas worldwide (Rogers et al., 2022), which can further exacerbate the societal and environmental impacts.

Extreme events which occur simultaneously in remote regions can result in more complex and severe consequences than those isolated or not connected hazards (Raymond et al., 2020). The amplified impacts of heat extremes occurring simultaneously in different places globally can have particular cumulative and widespread effects: concurrent heat extremes in multiple breadbasket regions could greatly reduce global crop production, increase prices and even disrupt and endanger global food supply (Gaupp et al., 2020; Kornhuber et al., 2020; Tigchelaar et al., 2018). Widespread heat extremes increase the demand for electricity, which may strain power grids and energy systems, leading to power outages or brownouts (Jiang et al., 2024; Van Vliet et al., 2016). The strain on infrastructure also impacts transportation, water supply, and other critical services, amplifying the overall societal and economic impacts. Concurrent heat extremes, especially when accompanied by dry conditions, could cause multiple severe wildfires to occur at the same time, considerably limiting the capacity to coordinate mutual support for disaster mitigation efforts (Bloem et al., 2022; Ruffault et al., 2020; Shi & Touge, 2022). Given the widespread societal and environmental impacts of concurrent heat extremes and a need to better understand risks under future climate conditions, it is important to investigate the mechanisms underlying the spatial concurrence of heat extremes, especially in the Northern Hemisphere where billions of people are exposed to extreme heatwaves in recent decades (Chambers, 2020; Coffel et al., 2018).

Heat extremes are induced by a series of physical processes. Human-induced global warming has significantly shifted temperatures toward an increased probability of heat extremes (Calvin et al., 2023; Seo et al., 2020; Vogel et al., 2020; Wehrli et al., 2020). The frequency and intensity of heat extremes are projected to increase under continued greenhouse gas emissions (AghaKouchak et al., 2014; Raymond et al., 2022). The occurrence of heat extremes is often linked to stationary high-pressure systems, also known as anticyclones. High-pressure systems, which are usually associated with jet streams and planetary circulations, can result in sinking air that compresses and warms, inhibits cloud formation, and limits heat dissipation, causing increased temperatures and heat accumulation at the surface, ultimately leading to extreme high temperature over different regions at the same time (Barriopedro et al., 2023; Pezza et al., 2012; Pfahl & Wernli, 2012). Additionally, the persistence and slow movement of high-pressure systems allow for prolonged heat build-up, exacerbating the intensity and duration of heat extremes. While a high-pressure system is a prerequisite for the initiation of heat events, land-atmosphere interactions further amplify the intensity and persistence of heat extremes (Seneviratne et al., 2006, 2013). Increased temperature enhances terrestrial evapotranspiration and accelerate the depletion of soil moisture (SM). In turn, low SM reduces evaporative cooling and shifts the net radiation toward sensible heating, resulting in higher temperatures and occurrence of extreme heat events (Dirmeyer et al., 2021; Miralles et al., 2019; Zhou et al., 2019). Persistent SM deficit may also aggravate anticyclonic anomalies and maintain anticyclonic circulation (Yoon et al., 2023). These physical processes, that is, global warming, anomalous anticyclone, and SM-atmosphere feedbacks, play important roles in the initiation and amplification of many extreme heat events.

While local drivers of heat extremes have been studied in detail, the mechanisms that are associated with concurrent heat extremes in different parts of the world have attracted attention only recently. Several recent studies have investigated the spatial concurrence of temperature extremes and identified the impacts of natural climate variability and anthropogenic climate change (Barriopedro et al., 2023; Sarhadi et al., 2018). Vogel et al. (2019) compared the exceptional nature of the 2018 Northern Hemispheric heatwave using observed and simulated data and identified the dominant effect of anthropogenic climate change on hemispheric-scale heatwaves. Circumglobal teleconnections, such as anomalous circulation regimes, could also lead to concurrent heatwaves across the Northern Hemisphere (Cohen et al., 2014; Coumou et al., 2014). Stationary Rossby waves in the tropospheric jet stream have been suggested as an important mechanism driving concurrent heat extremes in the mid-latitudes (Kornhuber et al., 2020). Rogers et al. (2022) proposed a new perspective to attribute the concurrent heatwaves at remote regions to different horizontal atmospheric patterns and explored the trends in thermodynamic and atmosphere dynamical drivers of heatwaves across mid- to high-latitudes in the Northern Hemisphere. Zhou et al. (2023) showed widespread concurrence of temperature extremes globally in observations and model simulations and identified the effects of natural climate variability and anthropogenic forcing on concurrent temperature extremes. While these studies have identified possible mechanisms that are responsible for the spatial concurrence of heat extremes, the influence of various physical drivers on the concurrence of heat extremes has yet been diagnosed.

Our study aims to investigate the spatial concurrence of extreme heat events and evaluate the contributions of key driving mechanisms to concurrent heat extremes in the Northern Hemisphere. We used a statistical framework to test the significance and quantify the strength of spatial concurrence of heat extremes across land grid cells in the Northern Hemisphere during the period of 1950–2023. To identify the mechanisms, we assessed the influences of global warming, high atmospheric pressure represented by abnormally high geopotential height, and SM-atmosphere feedbacks on spatially concurrent heat extremes. These analyses enable a comprehensive understanding of the spatial pattern and physical drivers of concurrent heat extremes in the Northern Hemisphere.

2. Materials and Methods

2.1. ERA5 Reanalysis

We used near surface air temperature, mid-troposphere Geopotential height fields (GPH, 500 hPa), and root-zone soil moisture (SM, 0–100 cm) from the ERA5 reanalysis produced by the European Center for Medium-Range Weather Forecasts (ECMWF) during the period of 1950–2023. The ERA5 reanalysis, which represents the fifth generation of ECMWF atmospheric reanalysis, offers hourly data encompassing various atmospheric, terrestrial, and oceanic climate variables (Hersbach et al., 2020). This comprehensive data set covers the globe on a regular 0.25-degree latitude-longitude grid. To identify widespread and persistent heat extremes, we resampled the original data to a 2-degree grid scale and aggregated the hourly data to 5-day means. With a low temporal and spatial resolution, we could evaluate spatially concurrent heat extremes over different regions more effectively.

2.2. Definition of Heat Extremes

Summer heat extremes were identified based on near surface temperature fields on a pentad (5-day) scale during the warm season (May–September, Days 122–270 in a leap year or days 121–271 in a non-leap year). We removed the mean seasonal cycle calculated as the 74-year mean temperature for each pentad to obtain temperature anomalies. Following previous studies (White et al., 2023; Zhou et al., 2023), the 95th percentile of temperature anomalies was used to calculate the threshold for heat extremes for each grid cell. This percentile-based threshold allows us to evaluate the spatial concurrence of heat extremes over different regions (see Section 2.3). To identify the impact of global warming, we identified the heat extreme events based on the 95th percentile of temperature anomalies with and without the long-term temperature trend, which was estimated based on the 10-year moving mean temperature.

2.3. Concurrent Heat Extremes

Concurrent heat extremes are defined by their simultaneous occurrence across different grid cells/regions. While earlier studies used the multivariate extreme value theory to identify the spatial clustering of climate extremes (Bador et al., 2015; Bernard et al., 2013), this approach cannot directly measure the strength of spatial concurrence over different regions. Therefore, we used a statistical framework to estimate the probability of concurrent heat extremes at the grid cell and regional scales and hence evaluate the spatial concurrence of heat extremes for each grid cell/region pair (Zhou et al., 2023). The time series of temperature anomalies at two grid cells, T_i and T_j, are transformed into normalized ranks as t_i and t_j, respectively. The probability of concurrent heat extremes at the two grid cells, that is, $P(T_i, T_j)$, can be expressed as

$$P(T_i, T_j) = P(t_i > 0.95 \wedge t_j > 0.95),\ i \neq j \quad (1)$$

To test the significance of the spatial concurrence of heat extremes, that is, $P(T_i, T_j)$, we used the hypothesis testing as follows:

1. The null hypothesis: temperature anomalies T_i and T_j are independent; thus, the probability of concurrent heat extremes at the two grid cells for each pentad (p) equals 0.0025 (0.05×0.05).

$$p = P(t_i > 0.95 \wedge t_j > 0.95),\ i \neq j \quad (2)$$

2. The alternative hypothesis: the heat extremes at the two grid cells are positively dependent and hence $p > 0.0025$.
3. To test the null hypothesis, we count the number of pentads (m) of all assessed samples (n) that heat extremes co-occur at the two grid cells.
4. If we assume that the occurrence of heat extremes is independent for different periods, the number of concurrent extremes would follow the binomial distribution. The probability of concurrent heat extremes that occur m times in n samples:

$$P_m = \frac{n!}{m!(n-m)!} p^m q^{n-m},\ p = 0.0025,\ q = 0.9975 \tag{3}$$

5. Based on the probability density function of binomial distribution, if the concurrent heat extremes occur at least 11 times during the whole study period ($n = 2220$), the p-value would be less than 0.05, and we can reject the null hypothesis. Correspondingly, the co-occurrence of heat extremes at the two grid cells is significant with a confidence level of 95%. On the contrary, if we cannot reject the null hypothesis, the heat extremes do not significantly co-occur at the two grid cells.

For each pair of grid cells where heat extremes are tested to significantly co-occur, we standardized the concurrence probability of heat extremes ($P(T_i, T_j)$) relative to the probability when heat extremes occur independently ($p_0 = 0.0025$). The ratio of the two is called probability multiplication factor (PMF):

$$\mathrm{PMF}_{i,j} = \frac{P(T_i, T_j)}{p_0} \tag{4}$$

As $P(T_i, T_j)$ is larger than 11/2220 (0.005) when heat extremes co-occur significantly, the PMF of concurrent heat extremes is greater than 2.0 (0.005/0.0025).

We assessed the spatial concurrence strength of heat extremes for IPCC AR6 land regions (Iturbide et al., 2020). For each pair of land regions, PMF was first computed for each pair of grid cells in the two regions, and the mean PMF was then computed to represent the spatial concurrence strength of heat extremes at the regional scale.

$$\mathrm{PMF}_{R_m, R_n} = \frac{\overline{P(T_i, T_j)}}{p_0},\ i \epsilon R_m,\ j \epsilon R_n \tag{5}$$

where PMF_{R_m, R_n} represents the mean PMF for the region pair of R_m and R_n, and $\overline{P(T_i, T_j)}$ is the mean of $P(T_i, T_j)$ of grid cell pairs where heat extremes co-occur significantly, with the grid cell i from the land region R_m and the grid cell j from the land region R_n, respectively.

We also identified the latitudinal distribution of PMF by computing the mean PMF for grid cell pairs where heat extremes have significantly co-occurred within each 10-degree moving zonal band at a 2-degree increment. Similarly, the hemispheric mean PMF was computed across all grid cell pairs where heat extremes have significantly co-occurred in the Northern Hemisphere.

2.4. Driving Factors of Concurrent Heat Extremes

To explore the mechanisms of concurrent heat extremes, we assessed the impacts of global warming, abnormally high pressure, and SM-atmosphere feedbacks, which have been shown to be the main drivers of regional heat extremes in previous studies (Barriopedro et al., 2023; Pezza et al., 2012; Röthlisberger & Papritz, 2023; Seneviratne et al., 2013; Zhou et al., 2023). We first identified the influence of global warming on concurrent heat extremes. To do so, we used temperature anomalies with and without long-term trends to identify heat extremes for each grid cell. By comparing results from these two sets of heat extremes, we could isolate the impact of warming trends on the proportion of land grid cells experiencing heat extremes simultaneously and the spatial concurrence strength of heat extremes at different grid cells/regions during the study period.

We further explored the impacts of concurrent high pressure and SM-atmosphere feedbacks on the spatial concurrence probability of heat extremes without the warming trends. The 500 hPa GPH anomalies were used to identify high-pressure events. To calculate GPH anomalies, we first removed the seasonal cycle of GPH for each grid cell by subtracting the 74-year mean GPH. Additionally, we accounted for the influence of thermal expansion on the troposphere (C. He et al., 2024), by subtracting the 10-degree latitude moving average for each pentad from 1950 to 2023. This allows us to identify concurrent high-pressure extremes and their impacts on the spatial concurrence of heat extremes. The SM anomalies were computed by removing the 74-year mean seasonal cycle for each pentad and each grid cell. Given that heat extremes may be driven by the amplified impact of multiple factors which are not that extreme individually, we defined the high-pressure extremes and low SM extremes as pentad periods as higher than its 90th percentile (GPH) and lower than its 10th percentile (SM), respectively, at each grid cell. To assess the collective effect of high-pressure anomalies and SM-atmosphere feedbacks, we also considered high GPH or low SM together as an extreme event called GS:

$$P(\mathrm{GS}_i) = P\left(g_i > 0.9 \vee s_i < 0.1\right) \tag{6}$$

where g_i and s_i represent the normalized ranks of GPH anomalies (G_i) and SM anomalies (S_i), respectively, and $P(\mathrm{GS}_i)$ is the probability of extreme GS events at the grid cell i.

Given the complex mechanisms of extreme heat events over different regions, it is difficult to disentangle the effects of various mechanisms on current heat extremes. Therefore, we empirically assessed the impacts of high GPH or low SM (i.e., extreme GS) on heat extremes by analyzing whether extreme GS coincides with extreme high temperature. We calculated the conditional probabilities of extreme high GPH ($P(G_i|T_i)$), extreme low SM ($P(S_i|T_i)$), and extreme GS ($P(\mathrm{GS}_i|T_i)$) when high temperature occurs at the grid cell i to determine the proportion of heat extremes associated with these driving factors and evaluate their impacts. Similarly, we identified the extent to which the concurrence of these driving factors can explain the concurrence probability of heat extremes at two grid cells i and j. The conditional probability of concurrent extreme GS for the two grid cells i and j where heat extremes occur simultaneously ($P(\mathrm{GS}_i, \mathrm{GS}_j|T_i, T_j)$) can be expressed as

$$\begin{aligned} P(\mathrm{GS}_i, \mathrm{GS}_j|T_i, T_j) &= \frac{P(\mathrm{GS}_i, \mathrm{GS}_j, T_i, T_j)}{P(T_i, T_j)} \\ &= \frac{P\left(\left(g_i > 0.9 \vee s_i < 0.1\right) \wedge \left(g_j > 0.9 \vee s_j < 0.1\right) \wedge t_i > 0.95 \wedge t_j > 0.95\right)}{P(t_i > 0.95 \wedge t_j > 0.95)} \end{aligned} \tag{7}$$

where $P(\mathrm{GS}_i, \mathrm{GS}_j, T_i, T_j)$ represents the probability of concurrent heat extremes and GS extremes, and $P(T_i, T_j)$ the probability of concurrent heat extremes at the grid cells i and j. The conditional probabilities of concurrent extreme high GPH ($P(G_i, G_j|T_i, T_j)$) and concurrent extreme low SM ($P(S_i, S_j|T_i, T_j)$) can also be calculated to determine how much concurrent heat extremes at the two grid cells can be explained by concurrent high GPH or low SM events, respectively. The three conditional probabilities, that is, $P(G_i, G_j|T_i, T_j)$, $P(S_i, S_j|T_i, T_j)$, and $P(\mathrm{GS}_i, \mathrm{GS}_j|T_i, T_j)$, enable us to evaluate and compare the contributions of concurrent high GPH, low SM, and their combined effects on concurrent heat extremes.

3. Results

3.1. Increases in Concurrent Heat Extremes in Recent Decades

Figure 1 shows increasing concurrent heat extremes in the Northern Hemisphere from 1950 to 2023. The proportion of land grid cells experiencing concurrent heat extremes ranged from 0.65% to 28% in the warm season (May–September, pentad scale) during 1950–2023 (Figure 1a). The annual proportion, averaged across all pentads for each year, varies from 2% to 8% during 1950–1999, and increased sharply from 5% in 2000 to 17% in 2023 (Figure 1b). In particular, the maximum proportion (corresponding to the max pentad) of land grid cells increased at a rate of 0.3% per year in the 21st century and reached 28% for a 5-day period in September 2023 (Figure 1b), which indicates increasing risks of concurrent heat extremes in the Northern Hemisphere. Such increases in the maximum proportion also support previous findings that the spatial extent of extreme heat events have greatly increased since 1980 (Rogers et al., 2022).

10.1029/2024EF005256

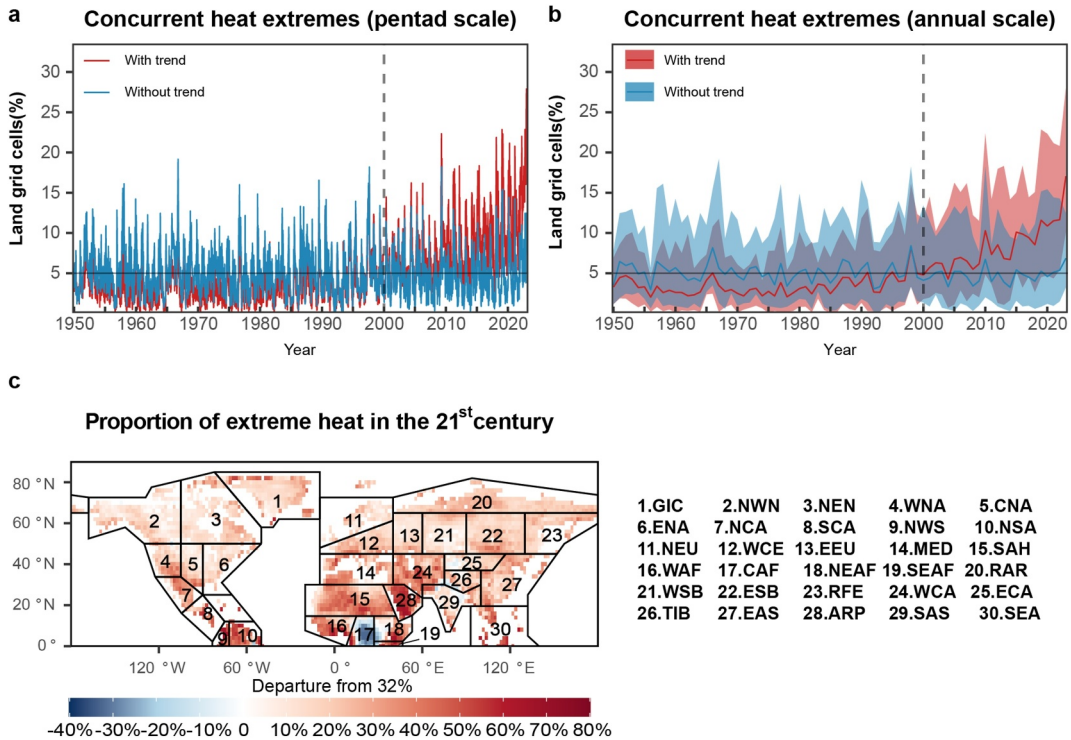

Figure 1. Increasing concurrent heat extremes in the Northern Hemisphere. (a) Proportion of land grid cells experiencing heat extremes in the warm season (May–September, pentad scale) during 1950–2023. The red and blue solid lines represent the proportions identified using temperature data with and without long-term trends. The gray solid line indicates the mean proportion (%) during the whole period while the gray dashed line shows the beginning of the 21st century. (b) The same as (a), but for the mean proportion of land grid cells experiencing heat extremes in each year. The upper and lower bounds of the shading shows the maximum and minimum proportions on the pentad scale for each year. (c) Departure in the proportion of heat extremes in the 21st century (2000–2023) from the expected proportion of 32% (i.e., 24 years in the 21st century/74 years in total) for the IPCC AR6 climate reference land regions. Blue and red colors show proportions of heat extremes lower and higher than the expected proportion of 32%, respectively.

A heat extreme threshold based on the 95th percentile results in a ratio of 5% of land grid cells, which are expected to experience concurrent heat extremes, assuming that heat extremes occur independently at different grid cells. Thus, any number higher or lower than a land coverage of 5% is due to the spatial concurrence of heat extremes. Further, the greater the departure from 5%, the stronger the concurrence strength of heat extremes. The increase in the mean proportion, and particularly the maximum proportion of heat extremes, suggest stronger concurrence strength of heat extremes that lead to the increase of concurrent heat extremes in the 21st century (Figures 1a and 1b).

The increase in the spatial concurrence of heat extremes is largely caused by global warming, which has led to more frequent and more intense heat extremes in the Northern Hemisphere, particularly in the 21st century (Robinson et al., 2021). Figure 1c shows that the proportion of heat extremes is much larger than the 32% (i.e., 24 years in the 21st century/74 years in total) over 96% of land grid cells and 29 of the 30 AR6 land regions in the Northern Hemisphere. With the long-term warming trends removed, we find both the mean and maximum proportions of land grid cells having concurrent heat extremes are greatly reduced from ∼8% and ∼17% with the warming trends to only ∼5% and ∼11% without in the 21st century (Figure 1b). Moreover, the trends in the mean and maximum proportions of concurrent heat extremes are insignificant (p-value > 0.05) without long-term warming trends. This demonstrates that the increasing frequency and strength of concurrent heat extremes are predominantly driven by the anthropogenic warming trends in the Northern Hemisphere.

3.2. Influence of Global Warming on Concurrent Heat Extremes

The concurrence of heat extremes is found to be significant across 24% of the grid cell pairs in the Northern Hemisphere, and their mean PMF is 3.09, 56% larger than the threshold of 2.0, that is, the minimum value for

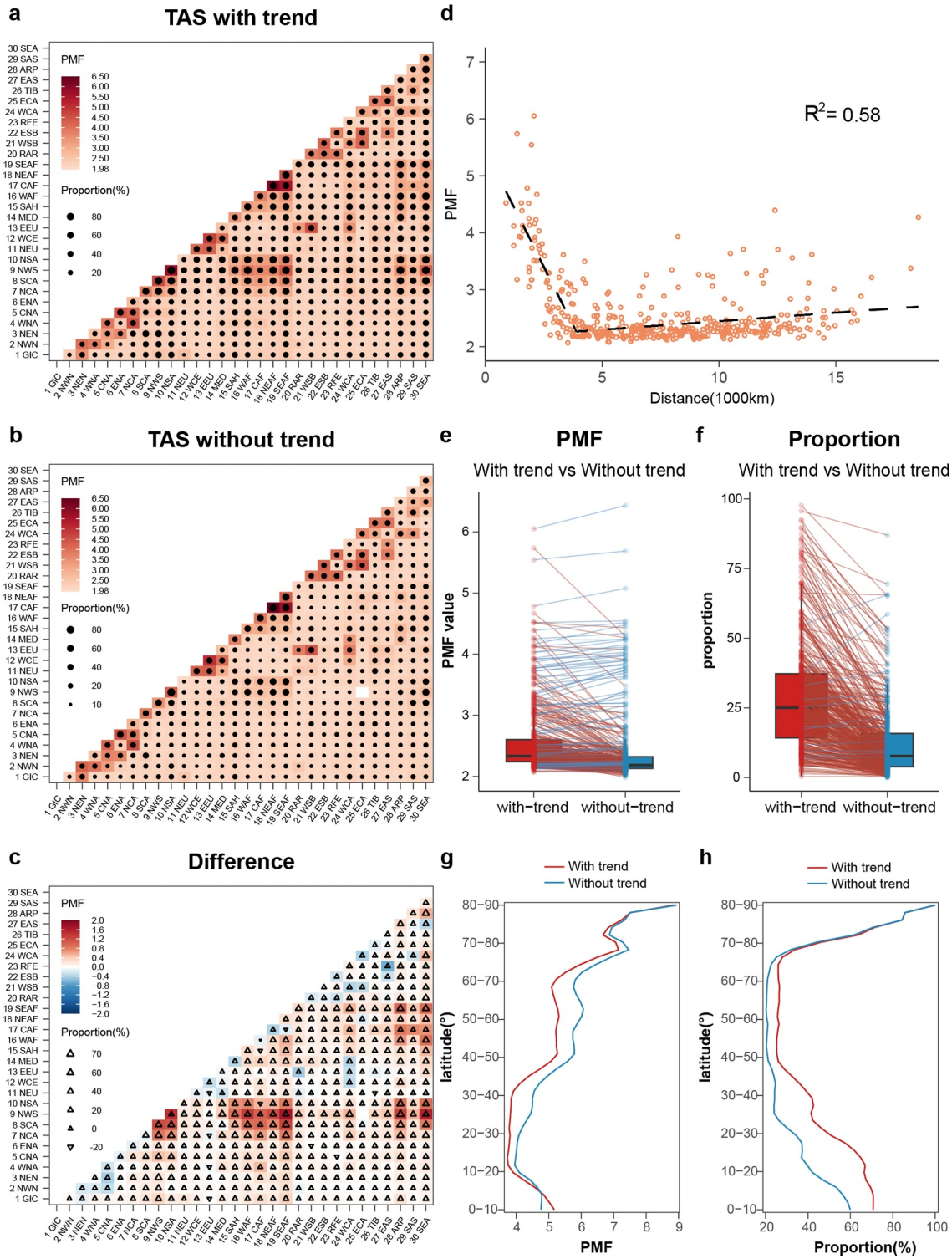

Figure 2. Global pattern of spatially concurrent heat extremes in the warm season based on the ERA5 reanalysis. (a) The mean probability multiplication factor (PMF) of concurrent heat extremes between AR6 land regions in the Northern Hemisphere. The dotted area shows the proportion of grid cell pairs where heat extremes are tested to be significantly concurrent for each AR6 region pair. (b) The same as a, but using near surface air temperature (TAS) data without long-term trends. (c) The effect of temperature trends on concurrent heat extremes evaluated as the difference between (a and b). (d) Changes in the regional PMF in a with the distance between the centers of each region pair. (e, f) Paired boxplots of the mean PMF and the proportion of land arid cells for each AR6 region pair shown in (a) (with TAS trend, red) and (b) (without TAS trend, blue). (g, h) Latitudinal distributions of the mean PMF and proportion of land grid cells for heat extremes within each 10-degree moving zonal band at a 2-degree increment.

statistical significance. This again indicates the spatial concurrence of heat extremes in the Northern Hemisphere. Figure 2a shows the concurrence strength of heat extremes across the 30 IPCC AR6 regions. The mean PMF across all regions (2.58, Figure 2e) is lower than the hemispheric mean PMF (3.09), as the former excludes grid cell pairs within each AR6 region, where PMF values are generally higher due to similar climatic conditions. The regional PMF is higher over neighboring regions, with the highest mean PMF of 6.05 across 66% of grid cell pairs between Central Africa (17CAF) and north Eastern Africa (18NEAF). High PMF is also detected across many distant regions (Figure 2d). For example, the mean PMF is 3.56 across 92% of grid cell pairs between northwestern South America (9NWS) and Arabian Peninsula (28ARP). The latitudinal patterns of the spatial concurrence of heat extremes are clearly evident (Figures 2g and 2h). As the grid cell pairs outside each 10-degree zonal band are excluded, the PMF values in Figure 2g are typically higher than the hemispheric mean PMF. The PMF and the proportion of grid cell pairs are largest in high-latitude regions that exhibit consistent Arctic climate features. We also find high PMF and proportion in the tropical regions (0–15°N). Indeed, the mean PMF and proportion are 3.80 ± 0.83 and $70\% \pm 23\%$, respectively, across the three tropical continents (Regions 8–10, 16–19, and 30) (Figure 2a). This result is consistent with previous findings that tropical land temperature shows strong spatial coherence, particularly when the Pacific Decadal Oscillation shifts to a warm phase, in recent decades (Yang et al., 2019; Zhou et al., 2023).

The identified strong concurrence strength of heat extremes in the Northern Hemisphere are largely driven by anthropogenic climate change. When the temperature trends are removed, the hemispheric mean PMF and proportion of concurrent heat extremes across statistically significant grid cell pairs are reduced from 3.09 to 2.41 and from 24% to 12%, respectively. We also find a lower PMF and smaller proportion over 84% and 97% of region pairs, respectively (Figures 2c, 2 e, and 2f). The reductions in PMF and proportion without the temperature trends are particularly strong across tropical regions (Regions 8–10, 16–19, and 30), indicating that the spatial concurrence of tropical heat extremes are strongly enhanced by the warming trends (Figures 2c, 2 g, and 2h). In mid- and high-latitude regions, the latitudinal patterns shift toward a higher proportion of grid cell pairs that are detected to experience significantly concurrent heat extremes, whose PMF value is close to the threshold 2.0, resulting in a lower mean PMF, when the warming trends are considered (Figures 2g and 2h). These results are consistent with the results of increased frequency and spatial extent of heat extremes in a warmer world (Figure 1) and confirmed that concurrent heat extremes have been greatly strengthened by global warming, particularly in the tropical regions.

3.3. Influences of Atmospheric Circulation and Land-Atmosphere Feedbacks on Concurrent Heat Extremes

While global warming has contributed to the strong spatial concurrence of heat extremes in the Northern Hemisphere, we also note widespread heat extremes and their spatial concurrence when the temperature trends have been removed (Figure 2). These concurrent heat extremes may be caused by natural climate variability and teleconnections, for example, the Rossby wave patterns which lead to concurrent high pressure in the mid-latitude regions (Kornhuber et al., 2020). To test this, we first identify the impact of abnormally high pressure on heat extremes for each grid cell. We find positive correlation between detrended temperature and GPH (Spearman's correlation coefficient = 0.54), indicating that high/low temperature are often associated with high/low GPH in the warm season (Figure 3d). The high probability (0.024) in the top-right bin of Figure 3d suggests that 48% (i.e., 0.024/0.05) of heat extremes, with a combined probability of 0.05, coincide with extreme high GPH on average. This proportion is relatively low (<30%) over most tropical regions, but much higher (56% on average) over 30–70°N (Figure 3a), indicating the importance of high pressure in mid-latitude heat extremes. While many studies also highlighted the importance of SM-atmosphere feedbacks in the intensification of extreme heat events (Miralles et al., 2014; Seneviratne et al., 2013), the negative correlation between temperature and SM is relatively weak (Spearman's correlation coefficient = −0.17) and only 21% of heat extremes co-occur with extreme low SM on average (Figures 3b and 3e). This suggests a secondary role of the SM-atmosphere feedbacks compared to the primary effect of high pressure in the occurrence of heat extremes in mid-latitude regions.

Combining the effects of high GPH and low SM as GS extremes (see Methods), 60% of heat extremes are accompanied by GS extremes on average, and the proportion is higher than this over more than half of the land grid cells in 12 of the 30 AR6 regions in mid-latitude regions (Figure 3c). Given the strong impact of GS extremes on regional heat extremes, we further examine whether concurrent GS extremes can explain concurrent heat extremes cross the 12 AR6 regions. For each region pair, 19%–61% (39% on average) of concurrent heat extremes

10.1029/2024EF005256

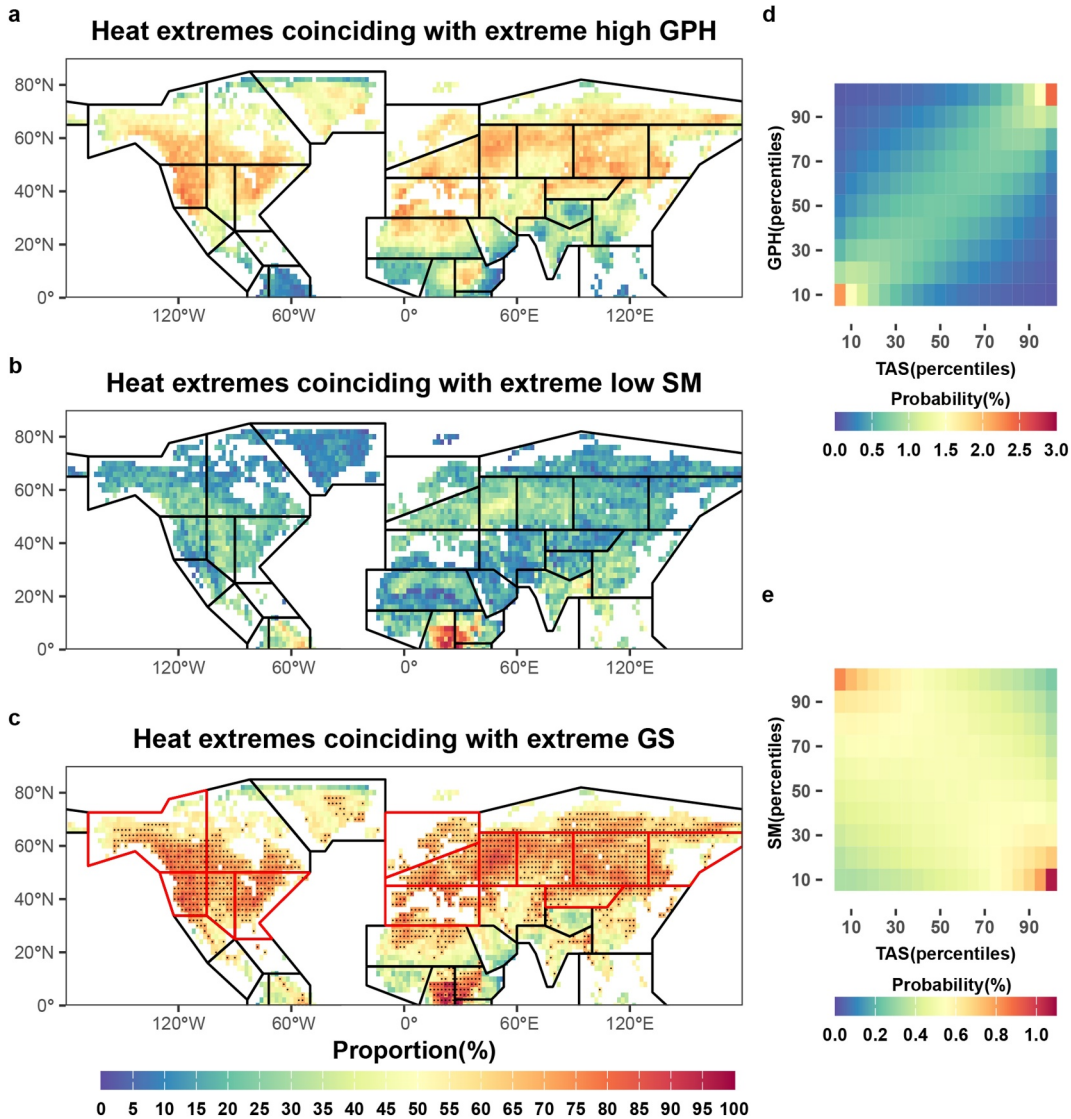

Figure 3. Heat extremes in relation to extreme high pressure and low soil moisture. (a–c) Proportion of heat extremes coinciding with extreme high geopotential height (GPH, a), extreme low soil moisture (SM, b), extreme high GPH or low SM (GS, c, see Equation 6) for each grid cell. (d, e) Mean probability of each percentile bin of near-surface air temperature (TAS) and GPH (d), SM (e), respectively, across all grid cells in the Northern Hemisphere. The long-term temperature trends have been removed to identify heat extremes, that is, above the 95th percentile of detrended TAS anomalies (the right column in d, e). The extreme high GPH and extreme low SM are defined as pentads in which the GPH anomalies are above their 90th percentile (the top row in d) and the SM anomalies below their 10th percentile (the bottom row in e), respectively. The black dots in (c) show grid cells where the proportion is larger than the average proportion of 60%. The red boundary lines show 12 AR6 regions in the mid-latitude regions where the proportion is higher than 60% over more than half of the land grid cells in each region.

are found to coincide with concurrent high GPH (Figure 4a). This suggests that abnormally high pressure are largely responsible for not only regional heat extremes but also concurrent heat extremes over different regions. In contrast, SM-atmosphere feedbacks only impact heat extremes at the regional scale and concurrent low SM plays a minor role in concurrent heat extremes, with the mean proportion of only 4% (Figure 4b). Combining the effects of high GPH and low SM in different regions, we find the concurrent GS extremes can explain 31%–69% (50% on average) of concurrent heat extremes. We note that this proportion is slight larger than the sum of concurrent high GPH and concurrent low SM (43%), as several concurrent heat extreme events are caused by high GPH at one grid cell and by low SM at the other grid cell.

10.1029/2024EF005256

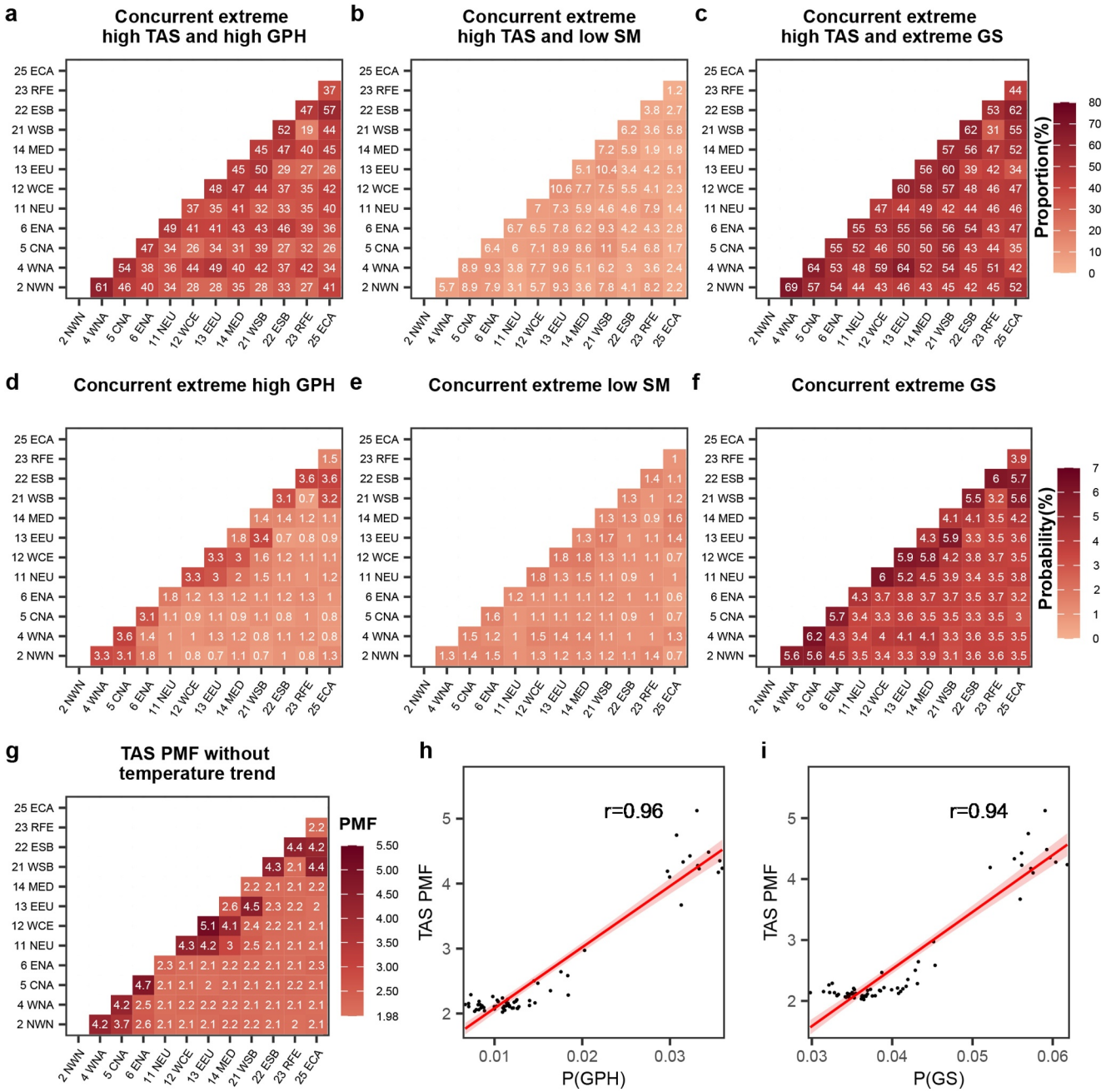

Figure 4. Impacts of concurrent high pressure and low SM on concurrent heat extremes in the warm season. (a–c) Proportion of concurrent high temperature (TAS, without trends) that coinciding with concurrent extreme high GPH (a), concurrent extreme low SM (b), and concurrent extreme GS (c, see Equation 7) at the 12 selected AR6 regions (grid cells with the proportion in Figure 3c larger than 60%). (d–f) The mean probability of concurrent high GPH (d), concurrent low SM (e), and concurrent extreme GS (f) for the grid cell pairs where heat extremes are tested to be significantly dependent (p-value < 0.05) between the 12 AR6 regions. (g) The mean PMF of concurrent heat extremes (without long-term temperature trends), but for the 12 AR6 regions. (h, i) The relationship between the PMF of concurrent heat extremes in g and the probability of concurrent GPH extremes in (d) (h) and concurrent GS extremes in (f) (i) across the 121 (12 × 11) region pairs. The standard deviation (regression line) and the Pearson's correlation coefficient are shown in each plot.

The analyses above demonstrate the importance of concurrent GS extremes in concurrent heat extremes in mid-latitude regions (Figure 4c). It remains unknown whether the high PMF of concurrent heat extremes is caused by the spatial concurrence of GS extremes, particularly extreme high GPH, across different region pairs. To test this, we calculated the mean probability of concurrent GS extremes for each region pair and find higher probability for the region pairs where the PMF of concurrent heat extremes is also higher (Figures 4d, 4 f, and 4g). The Pearson's

correlation coefficient between the PMF of concurrent heat extremes and the probability of concurrent GS extremes is 0.94 (Figure 4i), and this correlation coefficient is even higher (0.96) if we only considered concurrent high GPH (Figure 4h). This is because concurrent high GPH over different regions are interconnected through teleconnections, such as the Rossby wave patterns, but low SM generally depends on regional precipitation deficit and water loss through evapotranspiration and the probability of concurrent low SM are relatively low for all region pairs (Figure 4e). These results suggest that the spatial concurrence strength of heat extremes are predominantly driven by concurrent high-pressure anomalies. SM-atmosphere feedbacks mainly enhance regional heat extremes and could influence concurrent heat extremes in combination with high pressure over different regions.

4. Discussion and Conclusion

In this study, we developed a statistical framework to identify the contributions of global warming, atmospheric circulation and land-atmosphere feedbacks to spatial concurrence of heat extremes in the Northern Hemisphere. The statistical framework enables an evaluation of spatial concurrence strength of heat extremes between any grid cells or region pairs and at varying spatial scales. This approach overcomes the limitation of commonly used spatial clustering methods, which are unable to assess the strength of concurrent heat extremes over different regions (Bador et al., 2015; Bernard et al., 2013).

We find the direct effects of anthropogenic warming to be the dominant driver of long-term increases in the frequency and spatial extent of concurrent heat extremes in agreement with Rogers et al. (2022). The global warming trend also enhances the concurrence strength of heat extremes, particularly over tropical continents, where surface temperature has became more spatially coherent under climate warming (Yang et al., 2019; Zhou et al., 2023). In contrast, atmospheric circulation and land-atmosphere feedbacks primarily influence temporal (pentad-to-pentad, Figure 1) and spatial (across different region pairs, Figure 4) variations in concurrent heat extremes. Even when removing the warming trend, we find significant spatial concurrence of heat extremes across many regions, which is due to global climate teleconnections (Rouges et al., 2023; Ryu & Kang, 2023) and the size of heat extremes which might affect neighboring regions, such as the strong concurrence strength in high-latitude regions (Figures 2g and 2h). We find more than half of heat extremes in mid-latitude regions are associated with high-pressure extremes and 39% of concurrent heat extremes coincide with concurrent high-pressure extremes across 12 mid-latitude regions. Moreover, the spatial concurrence strength of heat extremes across mid-latitude region pairs strongly depends on the probability of concurrent high-pressure extremes ($r = 0.96$). Concurrent high-pressure extremes driven by large-scale circulation anomalies are therefore largely responsible for the spatial concurrence of heat extremes in mid-latitude regions. This finding is consistent with previous findings that mid-latitude heatwaves are connected by recurrent circulation patterns (Rogers et al., 2022), such as Rossby wave patterns with wavenumbers 5 and 7 (Ding & Wang, 2005; Kornhuber et al., 2019, 2020). While low soil moisture also enhances regional heat extremes through land-atmosphere feedbacks (Miralles et al., 2014, 2019; Zhou et al., 2019), it exerts its impact on co-occurring heat extremes over different regions primarily in combination with the high atmospheric pressure.

It is important to note that heat extremes can be triggered and modulated by various physical processes (Röthlisberger & Papritz, 2023). Concurrent heat extremes therefore may be caused by the same mechanism acting in different places or different processes occurring at the same time. Our statistical analyses assess how the three key mechanisms responsible for regional heat extremes, namely global warming, extreme high pressure, and SM-atmosphere feedbacks, contribute to concurrent heat extremes in different regions. However, the relative contributions of these mechanisms are not quantified due to their strong interconnection and the possibility that they are driven by the same or different physical processes. While we have isolated the global warming effect on temperature trends, global warming may also lead to amplified Rossby waves and hence more concurrent high-pressure anomalies and greater strength of concurrent heat extremes (Y. He et al., 2023; Kornhuber et al., 2020). In addition, other possible mechanisms of concurrent heat extremes, such as the El Niño–Southern Oscillation and related teleconnections (Jong et al., 2020; Mokhov & Timazhev, 2022), are not explicitly accounted for in this study, though they may have affected high-pressure anomalies and land-atmosphere feedbacks. A deeper understanding of the physical processes driving concurrent heat extremes, along with enhanced attribution analyses, is crucial for identifying the relative importance of different mechanisms and their interactions in the spatial concurrence of heat extremes, particularly in a warming future.

The identified strong influence of global warming on the spatial concurrence of heat extremes indicates ever-increasing risks of heat extremes in terms of not only its frequency and intensity but also its spatial extent. This would substantially increase heat exposure and heat-related mortality, and cause widespread damage to property and infrastructure and large-scale wildfire disasters (Arsad et al., 2022; Rey et al., 2009; Ruffault et al., 2020; Williams et al., 2019). While the increasing heat extremes pose adaptation challenges for the society and ecosystems, our improved understanding of the spatial pattern of concurrent heat extremes and their responses to different driving factors will inform effective strategies and practices to mitigate and adapt to future risks of heat extremes.

Data Availability Statement

The ERA5 reanalysis product is publicly available from https://cds.climate.copernicus.eu/datasets/reanalysis-era5-single-levels?tab=overview.

Acknowledgments
We acknowledge the Copernicus Climate Change Service, which is operated by the European Center for Medium-Range Weather Forecasts (ECMWF) on behalf of the European Union, for generating and distributing the ERA5 reanalysis data set (https://doi.org/10.24381/cds.adbb2d47). This work was supported by the National Key Research and Development Program of China (2022YFF0802401), the NSFC Excellent Young Scientists Fund (Overseas), and the Fundamental Research Funds for the Central Universities.

References

AghaKouchak, A., Cheng, L., Mazdiyasni, O., & Farahmand, A. (2014). Global warming and changes in risk of concurrent climate extremes: Insights from the 2014 California drought: Global warming and concurrent extremes. *Geophysical Research Letters*, *41*(24), 8847–8852. https://doi.org/10.1002/2014GL062308

Arsad, F. S., Hod, R., Ahmad, N., Ismail, R., Mohamed, N., Baharom, M., et al. (2022). The impact of heatwaves on mortality and morbidity and the associated vulnerability factors: A systematic review. *International Journal of Environmental Research and Public Health*, *19*(23), 16356. https://doi.org/10.3390/ijerph192316356

Bador, M., Naveau, P., Gilleland, E., Castellà, M., & Arivelo, T. (2015). Spatial clustering of summer temperature maxima from the CNRM-CM5 climate model ensembles & E-OBS over Europe. *Weather and Climate Extremes*, *9*, 17–24. https://doi.org/10.1016/j.wace.2015.05.003

Barriopedro, D., García-Herrera, R., Ordóñez, C., Miralles, D. G., & Salcedo-Sanz, S. (2023). Heat waves: Physical understanding and scientific challenges. *Reviews of Geophysics*, *61*(2), e2022RG000780. https://doi.org/10.1029/2022RG000780

Bastos, A., Ciais, P., Friedlingstein, P., Sitch, S., Pongratz, J., Fan, L., et al. (2020). Direct and seasonal legacy effects of the 2018 heat wave and drought on European ecosystem productivity. *Science Advances*, *6*(24), eaba2724. https://doi.org/10.1126/sciadv.aba2724

Bernard, E., Naveau, P., Vrac, M., & Mestre, O. (2013). Clustering of maxima: Spatial dependencies among heavy rainfall in France. *Journal of Climate*, *26*(20), 7929–7937. https://doi.org/10.1175/JCLI-D-12-00836.1

Bloem, S., Cullen, A. C., Mearns, L. O., & Abatzoglou, J. T. (2022). The role of international resource sharing arrangements in managing fire in the face of climate change. *Fire*, *5*(4), 88. https://doi.org/10.3390/fire5040088

Calvin, K., Dasgupta, D., Krinner, G., Mukherji, A., Thorne, P. W., Trisos, C., et al. (2023). IPCC, 2023: Climate Change 2023: Synthesis Report. In Core Writing Team, H. Lee, & J. Romero (Eds.), *Contribution of Working Groups I, II and III to the Sixth Assessment Report of the Intergovernmental Panel on Climate Change* (pp. 35–115). Intergovernmental Panel on Climate Change (IPCC). https://doi.org/10.59327/IPCC/AR6-9789291691647

Chambers, J. (2020). Global and cross-country analysis of exposure of vulnerable populations to heatwaves from 1980 to 2018. *Climatic Change*, *163*(1), 539–558. https://doi.org/10.1007/s10584-020-02884-2

Coffel, E. D., Horton, R. M., & De Sherbinin, A. (2018). Temperature and humidity based projections of a rapid rise in global heat stress exposure during the 21st century. *Environmental Research Letters*, *13*(1), 014001. https://doi.org/10.1088/1748-9326/aaa00e

Cohen, J., Screen, J. A., Furtado, J. C., Barlow, M., Whittleston, D., Coumou, D., et al. (2014). Recent Arctic amplification and extreme mid-latitude weather. *Nature Geoscience*, *7*(9), 627–637. https://doi.org/10.1038/ngeo2234

Coumou, D., Petoukhov, V., Rahmstorf, S., Petri, S., & Schellnhuber, H. J. (2014). Quasi-resonant circulation regimes and hemispheric synchronization of extreme weather in boreal summer. *Proceedings of the National Academy of Sciences of the United States of America*, *111*(34), 12331–12336. https://doi.org/10.1073/pnas.1412797111

Ding, Q., & Wang, B. (2005). Circumglobal teleconnection in the Northern Hemisphere summer. *Journal of Climate*, *18*(17), 3483–3505. https://doi.org/10.1175/JCLI3473.1

Dirmeyer, P. A., Balsamo, G., Blyth, E. M., Morrison, R., & Cooper, H. M. (2021). Land-atmosphere interactions exacerbated the drought and heatwave over northern Europe during summer 2018. *AGU Advances*, *2*(2). https://doi.org/10.1029/2020AV000283

Domeisen, D. I. V., Eltahir, E. A. B., Fischer, E. M., Knutti, R., Perkins-Kirkpatrick, S. E., Schär, C., et al. (2023). Prediction and projection of heatwaves. *Nature Reviews Earth and Environment*, *4*(1), 36–50. https://doi.org/10.1038/s43017-022-00371-z

García-León, D., Casanueva, A., Standardi, G., Burgstall, A., Flouris, A. D., & Nybo, L. (2021). Current and projected regional economic impacts of heatwaves in Europe. *Nature Communications*, *12*(1), 5807. https://doi.org/10.1038/s41467-021-26050-z

Gaupp, F., Hall, J., Hochrainer-Stigler, S., & Dadson, S. (2020). Changing risks of simultaneous global breadbasket failure. *Nature Climate Change*, *10*(1), 54–57. https://doi.org/10.1038/s41558-019-0600-z

He, C., Chen, X., Collins, M., Song, F., Hu, Y., Jiang, X., et al. (2024). Rising geopotential height under global warming. *Climate Dynamics*, *62*, 5769–5786. https://doi.org/10.1007/s00382-024-07175-5

He, Y., Zhu, X., Sheng, Z., & He, M. (2023). Resonant waves play an important role in the increasing heat waves in Northern Hemisphere mid-latitudes under global warming. *Geophysical Research Letters*, *50*(14), e2023GL104839. https://doi.org/10.1029/2023GL104839

Hersbach, H., Bell, B., Berrisford, P., Hirahara, S., Horányi, A., Muñoz-Sabater, J., et al. (2020). The ERA5 global reanalysis. *Quarterly Journal of the Royal Meteorological Society*, *146*(730), 1999–2049. https://doi.org/10.1002/qj.3803

Iturbide, M., Gutiérrez, J. M., Alves, L. M., Bedia, J., Cerezo-Mota, R., Cimadevilla, E., et al. (2020). An update of IPCC climate reference regions for subcontinental analysis of climate model data: Definition and aggregated datasets. *Earth System Science Data*, *12*(4), 2959–2970. https://doi.org/10.5194/essd-12-2959-2020

Jiang, L., Yang, Y., Wu, Q., Yang, L., & Yang, Z. (2024). Hotter days, dirtier air: The impact of extreme heat on energy and pollution intensity in China. *Energy Economics*, *130*, 107291. https://doi.org/10.1016/j.eneco.2023.107291

Jong, B.-T., Ting, M., Seager, R., & Anderson, W. B. (2020). ENSO teleconnections and impacts on U.S. summertime temperature during a multiyear La Niña Life cycle. *Journal of Climate*, *33*(14), 6009–6024. https://doi.org/10.1175/JCLI-D-19-0701.1

Kornhuber, K., Coumou, D., Vogel, E., Lesk, C., Donges, J. F., Lehmann, J., & Horton, R. M. (2020). Amplified Rossby waves enhance risk of concurrent heatwaves in major breadbasket regions. *Nature Climate Change*, *10*(1), 48–53. https://doi.org/10.1038/s41558-019-0637-z

Kornhuber, K., Osprey, S., Coumou, D., Petri, S., Petoukhov, V., Rahmstorf, S., & Gray, L. (2019). Extreme weather events in early summer 2018 connected by a recurrent hemispheric wave-7 pattern. *Environmental Research Letters*, *14*(5), 054002. https://doi.org/10.1088/1748-9326/ab13bf

Lüthi, S., Fairless, C., Fischer, E. M., Scovronick, N., Ben, A., Coelho, M. D. S. Z. S., et al. (2023). Rapid increase in the risk of heat-related mortality. *Nature Communications*, *14*(1), 4894. https://doi.org/10.1038/s41467-023-40599-x

Miralles, D. G., Gentine, P., Seneviratne, S. I., & Teuling, A. J. (2019). Land–atmospheric feedbacks during droughts and heatwaves: State of the science and current challenges. *Annals of the New York Academy of Sciences*, *1436*(1), 19–35. https://doi.org/10.1111/nyas.13912

Miralles, D. G., Teuling, A. J., van Heerwaarden, C. C., & Vilà-Guerau de Arellano, J. (2014). Mega-heatwave temperatures due to combined soil desiccation and atmospheric heat accumulation. *Nature Geoscience*, *7*(5), 345–349. https://doi.org/10.1038/ngeo2141

Mokhov, I. I., & Timazhev, A. V. (2022). Seasonal temperature extremes in the north Eurasian regions depending on ENSO phase transitions. *Atmosphere*, *13*(2), 249. https://doi.org/10.3390/atmos13020249

Perkins-Kirkpatrick, S. E., & Lewis, S. C. (2020). Increasing trends in regional heatwaves. *Nature Communications*, *11*(1), 3357. https://doi.org/10.1038/s41467-020-16970-7

Pezza, A. B., van Rensch, P., & Cai, W. (2012). Severe heat waves in Southern Australia: Synoptic climatology and large scale connections. *Climate Dynamics*, *38*(1), 209–224. https://doi.org/10.1007/s00382-011-1016-2

Pfahl, S., & Wernli, H. (2012). Quantifying the relevance of atmospheric blocking for co-located temperature extremes in the Northern Hemisphere on (sub-)daily time scales: Blocking and temperature extremes. *Geophysical Research Letters*, *39*(12), L12807. https://doi.org/10.1029/2012GL052261

Raymond, C., Horton, R. M., Zscheischler, J., Martius, O., AghaKouchak, A., Balch, J., et al. (2020). Understanding and managing connected extreme events. *Nature Climate Change*, *10*(7), 611–621. https://doi.org/10.1038/s41558-020-0790-4

Raymond, C., Suarez-Gutierrez, L., Kornhuber, K., Pascolini-Campbell, M., Sillmann, J., & Waliser, D. E. (2022). Increasing spatiotemporal proximity of heat and precipitation extremes in a warming world quantified by a large model ensemble. *Environmental Research Letters*, *17*(3), 035005. https://doi.org/10.1088/1748-9326/ac5712

Rey, G., Fouillet, A., Bessemoulin, P., Frayssinet, P., Dufour, A., Jougla, E., & Hémon, D. (2009). Heat exposure and socio-economic vulnerability as synergistic factors in heat-wave-related mortality. *European Journal of Epidemiology*, *24*(9), 495–502. https://doi.org/10.1007/s10654-009-9374-3

Robinson, A., Lehmann, J., Barriopedro, D., Rahmstorf, S., & Coumou, D. (2021). Increasing heat and rainfall extremes now far outside the historical climate. *npj Climate and Atmospheric Science*, *4*(1), 45. https://doi.org/10.1038/s41612-021-00202-w

Rogers, C. D. W., Kornhuber, K., Perkins-Kirkpatrick, S. E., Loikith, P. C., & Singh, D. (2022). Sixfold increase in historical Northern Hemisphere concurrent large heatwaves driven by warming and changing atmospheric circulations. *Journal of Climate*, *35*(3), 1063–1078. https://doi.org/10.1175/JCLI-D-21-0200.1

Röthlisberger, M., & Papritz, L. (2023). Quantifying the physical processes leading to atmospheric hot extremes at a global scale. *Nature Geoscience*, *16*(3), 210–216. https://doi.org/10.1038/s41561-023-01126-1

Rouges, E., Ferranti, L., Kantz, H., & Pappenberger, F. (2023). European heatwaves: Link to large-scale circulation patterns and intraseasonal drivers. *International Journal of Climatology*, *43*(7), 3189–3209. https://doi.org/10.1002/joc.8024

Ruffault, J., Curt, T., Moron, V., Trigo, R. M., Mouillot, F., Koutsias, N., et al. (2020). Increased likelihood of heat-induced large wildfires in the Mediterranean Basin. *Scientific Reports*, *10*(1), 13790. https://doi.org/10.1038/s41598-020-70069-z

Ryu, J.-H., & Kang, S.-L. (2023). Teleconnections link to summer heat extremes in the south-central U.S.: Insights from CMIP5 and CMIP6 simulations. *Weather and Climate Extremes*, *42*, 100635. https://doi.org/10.1016/j.wace.2023.100635

Sarhadi, A., Ausín, M. C., Wiper, M. P., Touma, D., & Diffenbaugh, N. S. (2018). Multidimensional risk in a nonstationary climate: Joint probability of increasingly severe warm and dry conditions. *Science Advances*, *4*(11), eaau3487. https://doi.org/10.1126/sciadv.aau3487

Seneviratne, S. I., Lüthi, D., Litschi, M., & Schär, C. (2006). Land–atmosphere coupling and climate change in Europe. *Nature*, *443*(7108), 205–209. https://doi.org/10.1038/nature05095

Seneviratne, S. I., Wilhelm, M., Stanelle, T., Hurk, B., Hagemann, S., Berg, A., et al. (2013). Impact of soil moisture-climate feedbacks on CMIP5 projections: First results from the GLACE-CMIP5 experiment. *Geophysical Research Letters*, *40*(19), 5212–5217. https://doi.org/10.1002/grl.50956

Seo, E., Lee, M.-I., Schubert, S. D., Koster, R. D., & Kang, H.-S. (2020). Investigation of the 2016 Eurasia heat wave as an event of the recent warming. *Environmental Research Letters*, *15*(11), 114018. https://doi.org/10.1088/1748-9326/abbbae

Shi, K., & Touge, Y. (2022). Characterization of global wildfire burned area spatiotemporal patterns and underlying climatic causes. *Scientific Reports*, *12*(1), 644. https://doi.org/10.1038/s41598-021-04726-2

Sidhu, B. S. (2023). Likely impacts of the 2022 heatwave on India's wheat production. *Environmental Research Letters*, *18*(10), 105001. https://doi.org/10.1088/1748-9326/acf871

Song, J., Zhou, S., Yu, B., Li, Y., Liu, Y., Yao, Y., et al. (2024). Serious underestimation of reduced carbon uptake due to vegetation compound droughts. *npj Climate and Atmospheric Science*, *7*(1), 23. https://doi.org/10.1038/s41612-024-00571-y

Thompson, V., Kennedy-Asser, A. T., Vosper, E., Lo, Y. T. E., Huntingford, C., Andrews, O., et al. (2022). The 2021 western North America heat wave among the most extreme events ever recorded globally. *Science Advances*, *8*(18), eabm6860. https://doi.org/10.1126/sciadv.abm6860

Tigchelaar, M., Battisti, D. S., Naylor, R. L., & Ray, D. K. (2018). Future warming increases probability of globally synchronized maize production shocks. *Proceedings of the National Academy of Sciences of the United States of America*, *115*(26), 6644–6649. https://doi.org/10.1073/pnas.1718031115

Van Vliet, M. T. H., Wiberg, D., Leduc, S., & Riahi, K. (2016). Power-generation system vulnerability and adaptation to changes in climate and water resources. *Nature Climate Change*, *6*(4), 375–380. https://doi.org/10.1038/nclimate2903

Vogel, M. M., Zscheischler, J., Fischer, E. M., & Seneviratne, S. I. (2020). Development of future heatwaves for different hazard thresholds. *Journal of Geophysical Research: Atmospheres*, *125*(9), e2019JD032070. https://doi.org/10.1029/2019JD032070

Vogel, M. M., Zscheischler, J., Wartenburger, R., Dee, D., & Seneviratne, S. I. (2019). Concurrent 2018 hot extremes across Northern Hemisphere due to human-induced climate change. *Earth's Future*, *7*(7), 692–703. https://doi.org/10.1029/2019EF001189

Wehrli, K., Hauser, M., & Seneviratne, S. I. (2020). Storylines of the 2018 Northern Hemisphere heatwave at pre-industrial and higher global warming levels. *Earth System Dynamics*, *11*(4), 855–873. https://doi.org/10.5194/esd-11-855-2020

White, R. H., Anderson, S., Booth, J. F., Braich, G., Draeger, C., Fei, C., et al. (2023). The unprecedented Pacific Northwest heatwave of June 2021. *Nature Communications*, *14*(1), 727. https://doi.org/10.1038/s41467-023-36289-3

Williams, A. P., Abatzoglou, J. T., Gershunov, A., Guzman-Morales, J., Bishop, D. A., Balch, J. K., & Lettenmaier, D. P. (2019). Observed impacts of anthropogenic climate change on wildfire in California. *Earth's Future*, *7*(8), 892–910. https://doi.org/10.1029/2019EF001210

Xu, W., Yuan, W., Wu, D., Zhang, Y., Shen, R., Xia, X., et al. (2024). Impacts of record-breaking compound heatwave and drought events in 2022 China on vegetation growth. *Agricultural and Forest Meteorology*, *344*, 109799. https://doi.org/10.1016/j.agrformet.2023.109799

Yang, H., Piao, S., Huntingford, C., Peng, S., Ciais, P., Chen, A., et al. (2019). Strong but intermittent spatial covariations in tropical land temperature. *Geophysical Research Letters*, *46*(1), 356–364. https://doi.org/10.1029/2018GL080463

Yoon, D., Kang, T., Cha, D., Song, C., Lee, M., Min, K., et al. (2023). Role of land–atmosphere interaction in the 2016 Northeast Asia heat wave: Impact of soil moisture initialization. *Journal of Geophysical Research: Atmospheres*, *128*(2), e2022JD037718. https://doi.org/10.1029/2022JD037718

Zhou, S., Williams, A. P., Berg, A. M., Cook, B. I., Zhang, Y., Hagemann, S., et al. (2019). Land–atmosphere feedbacks exacerbate concurrent soil drought and atmospheric aridity. *Proceedings of the National Academy of Sciences of the United States of America*, *116*(38), 18848–18853. https://doi.org/10.1073/pnas.1904955116

Zhou, S., Yu, B., & Zhang, Y. (2023). Global concurrent climate extremes exacerbated by anthropogenic climate change. *Science Advances*, *9*(10), eabo1638. https://doi.org/10.1126/sciadv.abo1638